

Processing Specular Reflection Components of Chrome-plated Surface by Multi-Image Reconstruction Method

Chang Jiang LI^{1,2}, Zhong ZHANG¹, Tetsuo MIYAKI¹, Takashi IMAMURA¹ and Hisanaga FUJIWA³

¹Instrumentation Systems Lab, Dept. of Production Systems Engineering
Toyohashi University of Technology, 441-8580, Japan
zhang@is.pse.tut.ac.jp

²Dept. of Mechanical and Engineering,
²Chongqing University of Science and Technology, Chongqing, PR. China, 400042
li@is.pse.tut.ac.jp

³Industrial Technology Center, Okayama Prefecture
Okayama, 701-1296, Japan

Abstract: Chrome-plated surfaces are perfectly specular, in which the diffuse reflection components are weak while the specular reflection components are so strong that their intensities saturate the CCD matrix and cause some surface features to be lost. This situation means that one image alone cannot show all of the surface features. To process specular reflection components, we proposed a novel multi-image reconstruction method (MIRM), which reconstructs a synthetic image from a set of images. In the set of images that are captured by a special ring pattern illumination system, the specular spots move in a smooth motion in the intact surface as the light source moves, and new gradient values can be obtained. Using the new gradient values a synthetic image can be reconstructed by the multi-grid method. Experimental results show that our method is effective in significantly removing specular highlights, while preserving or sharpening such features as edges and defects.

Keywords: specular reflection; diffuse reflection; chrome-plated surface; multi-image reconstruction.

1. Introduction

The reflection of light from surfaces is generally classified into two main categories: diffuse reflection and specular reflection. The specular component is a surface phenomenon, often concentrating in a compact lobe and causing strong highlights to appear in the image. In the reflected light from smooth metallic surfaces, the specular reflection component is very strong while the diffuse reflection components are too weak, although the diffuse reflection components include some useful information for surface inspection. In most cases, these highlights can cause many algorithms for segmentation and surface inspection to produce erroneous results. In classical computer vision algorithms the influence of the highlight spots is not fully considered, and the object's surface is always assumed to be Lambertian. Therefore, automatic inspection of a variety of defects on smooth metallic surfaces, such as polished metal parts and chrome-plated surfaces, is very difficult.

The removal of specular components is an essential step in obtaining the correct information from images, otherwise

errors are inevitable. Various methods for identifying and removing specular reflection components have been developed. Moreover, most of them have been applied to inhomogeneous objects. Wolff and Boult [1] used a polarizing filter to separate reflection components from a gray image. The basic idea is that, for most incident angles, diffuse reflection tends to be less polarized than specular reflection. Nayar et al. [2] extended the method above by considering a combination of polarizing filters and colors. A specular pixel has a different intensity if the polarization angle of the filter is changed. This method can be used for textured surfaces, but is impractical in some circumstances because of the additional filters. Sato and Ikeuchi [3] introduced a four-dimensional space to analyze the diffuse and specular reflection components based on colors and image intensity. This method has the ability to separate the reflection components locally, but it requires dense input images with variation in illuminant directions. Tan and Ikeuchi [4] proposed a specular-to-diffuse mechanism which is based solely on colors, particularly chromaticity, without requiring any geometrical information. However, there are quite a few methods for processing specular highlights of such perfectly specular surfaces as Chrome-plated surfaces. Some of the current techniques for measuring metal surfaces even require painting the surface with powder, which slows measurement speed and reduces measurement accuracy. Rogerio Feris [5] proposed a method which is based on Multi-flash images. Mukaigawa [6] proposed a photometric linearization method (PLM) that converts input images including various photometric factors into ones that include only a diffuse factor. This method cannot work stably when some pixels are not illuminated in many input images although it is a useful method for removing specular reflection components from the reflected light. Zhang et al. [7] presented a special random sampling method (SRSF). In this method, a set of images taken in various lighting conditions are converted successfully into synthetic images that contain only diffuse reflection components. Twenty images are taken in different light source directions, so it takes a much longer time to finish the

processing. This limits its real-world applicability.

On smooth metallic surfaces, the specular reflection component is not only so strong that it saturates the camera processing unit, but it also accounts for a considerable area in the image. The highlight spots make many useful features, such as edges, defects, and hidden information. This means that by only processing one image it is not possible to obtain all of the surface information. In this case, the method above cannot be applied to smooth metallic surfaces. Therefore, we investigate the illuminant system based on discussing the reflection model on Chrome-plated surfaces and capture a set of images with different incidence light directions, which can describe the whole surface information. In addition, we propose a multi-image reconstruction method (MIRM) to process these images for reconstructing a synthetic image, in which not only specular reflection components are significantly reduced, but also all defects are integrated and the complete surface information is presented. Some experiments for chrome-plated Acrylonitrile Butadiene Styrene (ABS) resin were carried out by using our experiment system. The initial results show that the method is feasible for chrome-plated surfaces.

The remainder of the paper is organized as follows. We will discuss the reflection model on Chrome-plated Surface in the next section and present our method in section 3. In section 4, the illumination system is described in detail. We show some experiment results in section 5 and finally, the paper is concluded in section 6.

2. Review of the Reflection Model

Reflection off metallic surfaces is different from that off inhomogeneous surfaces. In the case of an inhomogeneous (dielectric) material, the following four reflected light elements shown in Fig.1 have been considered [8]:

1. Specular reflection that reflects once off a surface which is flatter than the wavelength of the incident light.
2. Diffuse reflection that has reflected two or more times off a rough surface, which consists of material smaller in size than the wavelength of the incident light.
3. Diffuse reflection that diffracted on the surface, which consists of material not greater in size than the wavelength of the incident light. Usually, the reflected light element can almost be disregarded because it is very small except when the surface of the object has a periodic structure of order roughly equivalent to the wavelength of the light.
4. Diffuse reflection that first penetrated the surface, and then escaped the surface after a repetition of reflections off colored matter (pigment) on the inside of the dielectric material.

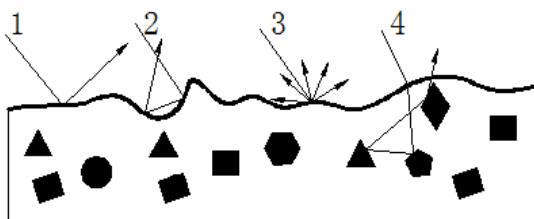


Fig.1 Reflection of light off a dielectric material

In the reflected light off a metallic material there is no fourth element. This is because the metallic material has conductive electrons, so the electric field of the light is covered by Dolude’s Law and the light cannot enter the metal. Furthermore, reflection off a metallic surface is different from that off a dielectric surface. For one thing, the reflections have different polarization properties. For unpolarized incident light, the reflected light off a metallic surface is still unpolarized, while the reflected light off an inhomogeneous surface is polarized. A second reason is that for smooth metallic surfaces, specular reflection is very strong and diffuse reflection is too weak. Moreover, the surroundings are often observed as specular reflections.

On the other hand, Nayar et al. [9] proposed a reflectance framework for smooth and rough metallic surfaces. The model is comprised of three reflection components: the diffuse lobe I_{dl} , the specular lobe I_{sl} , and the specular spike I_{ss} . These three components are shown in Fig.2 and the coordinate system used for the model is shown in Fig.3.

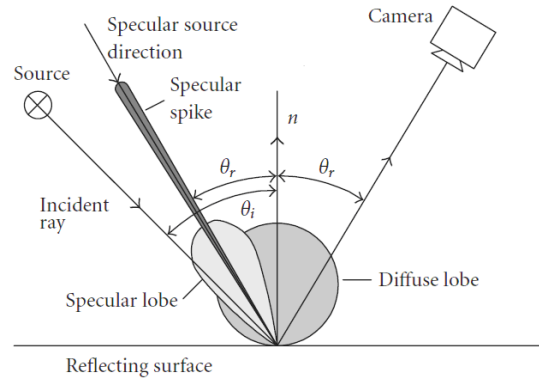


Fig.2 The reflection model [9]

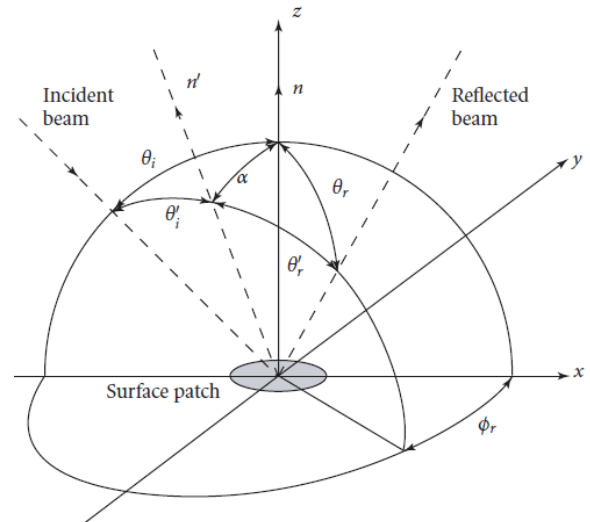


Fig.3 Coordinate system for the reflection model [10]

As is shown in Fig.3, the light reflected from the surface in the direction of the camera causes an image with the intensity [9]

$$I_k = I_{dl} + I_{sl} + I_{ss}, \quad (1)$$

where each reflectance component can be shown as follows:

(i) Diffuse lobe I_{dl} : the diffuse component is represented by the Lambertian model,

$$I_{dl} = K_{dl} \cos \theta_i, \quad (2)$$

where K_{dl} denotes the strength of the diffuse lobe, and θ_i is the angle of the incident light rays.

(ii) Specular lobe I_{sl} : a Torrance-Sparrow model [10] is used to predict the Specular lobe:

$$I_{sl} = K_{sl} \exp\left(-\frac{\alpha^2}{2\sigma_\alpha^2}\right) F(\theta'_i, \eta') G(\theta_i, \theta_r, \phi_r), \quad (3)$$

where K_{sl} is the magnitude of the specular lobe, $\exp(-\alpha^2/2\sigma_\alpha^2)$ is an exponential term that describes the slope distribution of the micro-facets assuming a normal distribution, α is the angle between the normal vector of the micro-facet \vec{n}' and the normal vector of the macro surface \vec{n} , that is $\alpha = \arccos(\vec{n}' \cdot \vec{n})$, and σ_α is the standard deviation of the surface height. Smaller values of σ_α indicate the surface is smoother ($\sigma_\alpha = 0$ represents a perfectly smooth surface, like a pure mirror). Larger values of σ_α imply the surface is rougher. $F(\theta', \eta')$, where θ' is the local angle of incidence and η' is the complex index of refraction, is the Fresnel coefficient, and under certain conditions it can be defined as a constant value. $G(\theta_i, \theta_r, \phi_r)$ is a geometric attenuation factor, and it describes the shadowing and masking effects of micro-facets by adjacent micro-facets. When the viewing direction coincides with the mean normal vector \vec{n} , the factor G equals unity over a large range of θ_i .

(iii) Specular spike I_{ss} : the specular spike component is a very sharp function, which is described by a delta function.

On the other hand, the surfaces roughness of Chrome-plated surfaces is very small and the specular lobe is more dominant than the specular spike. Optical measurement shows that diffuse reflection is very weak (see section 5) and no specular spike [11] was presented. Furthermore, the Fresnel coefficient of a smooth metallic surface is nearly constant. Hence, the reflectance model can be restricted in the specular lobe component to describe the change of the specular spot under different conditions. However, the defect always appears specular because of the change of the normal vector of the micro-facet. Therefore, the model proposed by Nayar et al. [9] suggests the configuration of an illumination system, and proposes a new method of processing images of specular reflection off Chrome-plated surfaces.

3. A New Approach of Processing Specular Reflection

In this section, we propose a new method for processing specular reflection components from smooth specular surfaces, such as Chrome-plated surfaces. The procedure of the proposed method is demonstrated in Fig.4.

First, we input a set of images taken with different lighting directions. Second, the intensity gradient of every input image taken with a certain light source direction is calculated. And then we get the new gradient image from all input images to eliminate the outliers. The new gradient image has to be padded so that its size is square in order to use the multi-grid

method. Third, using the multi-grid method, we reconstruct a synthetic image from the new gradient image. Last, we need to crop back the resulting image to its original size and output the image for future processing.

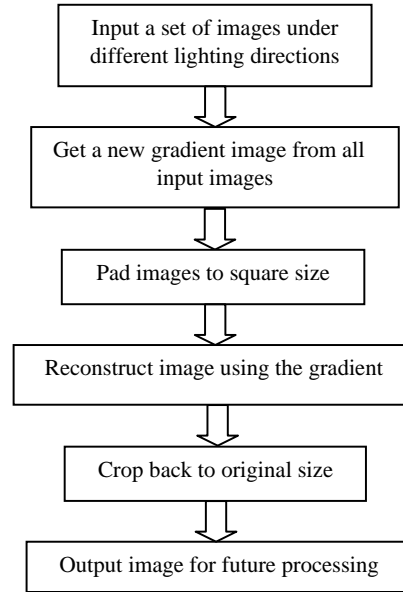


Fig.4 The procedure of the proposed method

3.1 The fundamental principle

The specular lobe component reflected off the Chrome-plated surfaces is dominant, as mentioned in section 2. Furthermore, the specular lobe component depends mainly on the direction of the light source and the normal direction of the impinged point if all other conditions remain unchanged, as shown in Fig.5[12]. It is obvious that when a light source moves smoothly, the specular spot reflected from the flawless smooth surface will move smoothly and gradually because of the continuity of the normal direction on the smooth surface.

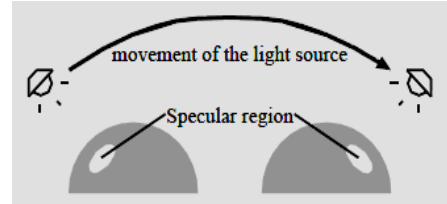


Fig.5 Specular spots shift as the light direction changes.

We capture a set of images, in which the azimuth angle of incidence light is varied while the elevation angle is kept constant. Let I_k ($1 \leq k \leq n$) be an image series, where I denotes the pixel intensity and sub-index k denotes the sequence number of the image taken with light source direction number k . If now a certain pixel (x, y) in all input images on the smooth surface is observed, we can find the course of the gradient variation of the pixel. If the gradient of the pixel (x, y) is the highest among all input images, the pixel is certainly at a specular boundary. On the other hand, if pixel (x, y) is in a specular region or in a shadow region, the gradient of the pixel will be close to 0, which is the lowest among all input images. Therefore, we can eliminate the specular pixel by combining the gradient value of the set of

images to get a new gradient image. We obtain the new gradient image by the following procedure.

1) Calculate the intensity gradient of every input image that is taken with a certain light source direction.

$$G_k(x, y) = \nabla I_k(x, y) = \begin{bmatrix} \frac{\partial I_k}{\partial x} \\ \frac{\partial I_k}{\partial y} \end{bmatrix}, \quad (4)$$

Where k is the image number ($k = 1, 2, \dots, n$), and ∇ is the gradient operator.

2) Get a new gradient image by weighted summation of the intensity gradients at the corresponding position in all input images, that is:

$$G(x, y) = \sum_k \lambda_k G_k(x, y) = \begin{bmatrix} G_x \\ G_y \end{bmatrix}, \quad (5)$$

Where λ_k is the weight of the image k , and G_x, G_y denotes the median gradient in directions x and y , respectively.

Some methods for deciding an optimum combination of series gradient images have been adapted on the basis of statistics analysis. In the paper, we select a simple method to get the new gradient image. The method is to find the median gradient value at the corresponding position in all input images. It is obvious that in the new gradient field, these outliers have been removed and only the gradient values of diffuse reflection components are present. It needs to be noted that the intensity of a pixel resulting from a defect part of the chrome-plated surface is similar to the specular components thanks to the sharp changing of its normal direction. In addition, these highlights result from a defect present in the same place in most of the series images although the size of the specular spot may differ slightly. It is evident that the processing method can remove specular reflection components resulting from an intact smooth surface, but results in the preservation of defect information.

3.2 Image Reconstruction

We need to reconstruct a synthetic image using the new gradient value obtained in the above process for future processing.

One first assumes the synthetic image \tilde{I} satisfies the equation

$$\nabla \tilde{I} = G(x, y), \quad (6)$$

and then the space of all 2D potential functions is searched for a function \tilde{I} whose gradient value is closest to G in the least-squares sense. In other words, the following integral value should be minimized:

$$\iint F(\nabla \tilde{I}, G) dx dy, \quad (7)$$

where $F(\nabla \tilde{I}, G) = \|\nabla \tilde{I} - G\|^2 = (\frac{\partial \tilde{I}}{\partial x} - G_x)^2 + (\frac{\partial \tilde{I}}{\partial y} - G_y)^2$.

According to the variation principle, the image \tilde{I} that minimizes the integral value in equation (7) must satisfy the Euler-Lagrange equation:

$$\frac{\partial F}{\partial \tilde{I}} - \frac{d}{dx} \frac{\partial F}{\partial \tilde{I}_x} - \frac{d}{dy} \frac{\partial F}{\partial \tilde{I}_y} = 0. \quad (8)$$

In fact, equation (8) is a partial differential equation in \tilde{I} .

Substituting F , we obtain the following equation:

$$2\left(\frac{\partial^2 \tilde{I}}{\partial x^2} - \frac{\partial G_x}{\partial x}\right) + 2\left(\frac{\partial^2 \tilde{I}}{\partial y^2} - \frac{\partial G_y}{\partial y}\right) = 0. \quad (9)$$

Then, we can get the Poisson equation:

$$\nabla^2 \tilde{I} = \text{div} G, \quad (10)$$

where $\nabla^2 \tilde{I} = \frac{\partial^2 \tilde{I}}{\partial x^2} + \frac{\partial^2 \tilde{I}}{\partial y^2}$, ∇^2 is the Laplacian operator, and

$\text{div} G = \frac{\partial G_x}{\partial x} + \frac{\partial G_y}{\partial y}$ is the divergence of the new gradient values G .

For a 2-D digital image of size $m \times n$, we use the multi-grid method to solve equation (10) and get the synthetic image. In order to satisfy the requirement of the method, we pad the images to make them square and of size N being a power of two. Lastly, the resulting image is cropped back to its original size.

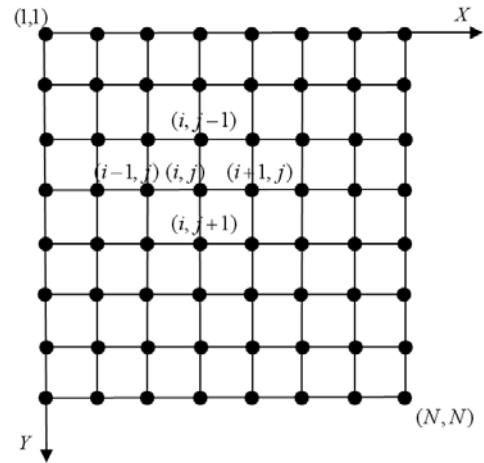


Fig.6 Two-dimensional grid

We can regard the image as a two-dimensional region Ω as shown in Fig.6, where each pixel is regarded as a grid node with an interval distance of h . Let $\tilde{I}(i, j)$ be the intensity of the pixel (i, j) in the reconstructed image \tilde{I} . By using the two-dimensional Taylor function, we can represent $\tilde{I}(i, j)$ as the following equation using the neighboring four pixels' intensities:

$$\begin{aligned} \tilde{I}_{i-1,j} &= \tilde{I}(i-h, j) \\ &= \tilde{I}_{i,j} - h \left(\frac{\partial \tilde{I}}{\partial x}\right)_{i,j} + \frac{h^2}{2} \left(\frac{\partial^2 \tilde{I}}{\partial x^2}\right)_{i,j} - O(h^3), \end{aligned} \quad (11)$$

$$\begin{aligned} \tilde{I}_{i+1,j} &= \tilde{I}(i+h, j) \\ &= \tilde{I}_{i,j} + h \left(\frac{\partial \tilde{I}}{\partial x}\right)_{i,j} + \frac{h^2}{2} \left(\frac{\partial^2 \tilde{I}}{\partial x^2}\right)_{i,j} + O(h^3), \end{aligned} \quad (12)$$

where $O(h^3)$ is the remainder term of third order. By adding equations (11) and (12), we can obtain the second-order partial derivatives $(\frac{\partial^2 \tilde{I}}{\partial x^2})_{i,j}$ in the x direction as follows:

$$\left(\frac{\partial^2 \tilde{I}}{\partial x^2}\right)_{i,j} = \frac{1}{h^2} (\tilde{I}_{i-1,j} - 2\tilde{I}_{i,j} + \tilde{I}_{i+1,j}). \quad (13)$$

In the same way, we can get the second-order partial

derivatives $(\frac{\partial^2 \tilde{I}}{\partial y^2})_{i,j}$ in the y direction:

$$(\frac{\partial^2 \tilde{I}}{\partial y^2})_{i,j} = \frac{1}{h^2} (\tilde{I}_{i,j-1} - 2\tilde{I}_{i,j} + \tilde{I}_{i,j+1}). \quad (14)$$

Let h be unit distance ($h=1$), and adding equations (13) and (14), we obtain the following equation:

$$\begin{aligned} \nabla^2 \tilde{I} &= \frac{\partial^2 \tilde{I}}{\partial x^2} + \frac{\partial^2 \tilde{I}}{\partial y^2} \\ &= \tilde{I}_{i+1,j} + \tilde{I}_{i-1,j} + \tilde{I}_{i,j+1} + \tilde{I}_{i,j-1} - 4\tilde{I}_{i,j}. \end{aligned} \quad (15)$$

Using a similar method, we can also represent $\text{div}G$ as in the following equation:

$$\begin{aligned} \text{div}G_{i,j} &= \frac{\partial G_{x_{i,j}}}{\partial x} + \frac{\partial G_{y_{i,j}}}{\partial y} \\ &= G_{x_{i,j}} - G_{x_{i-1,j}} + G_{y_{i,j}} - G_{y_{i,j-1}}. \end{aligned} \quad (16)$$

In order to solve equation (10), we need to convert the reconstructed image \tilde{I} to a matrix U in the direction y .

$$U = [\bar{u}_1, \bar{u}_2, \dots, \bar{u}_j, \dots, \bar{u}_{N-1}]^T, \quad (17)$$

where $\bar{u}_j = [\tilde{I}_{1,j}, \tilde{I}_{2,j}, \dots, \tilde{I}_{N-1,j}]^T$.

We can also convert $\text{div}G$ to a matrix Q in the direction y .

$$Q = [\bar{q}_1, \bar{q}_2, \dots, \bar{q}_j, \dots, \bar{q}_{N-1}]^T, \quad (18)$$

where $\bar{q}_j = -1/4 \cdot [\text{div}G_{1,j}, \text{div}G_{2,j}, \dots, \text{div}G_{N-1,j}]^T$.

Then, the linear equation shown in (19) can be obtained by substituting equations (15) ~ (18) into equation (10).

$$L^*U = Q, \quad (19)$$

where L is an order $(N-1)^2 \times (N-1)^2$ sparse matrix and can be shown as follows:

$$L = \begin{bmatrix} K & -E/4 & \dots & 0 \\ -E/4 & K & -E/4 \dots & \vdots \\ \vdots & \ddots & \ddots & -E/4 \\ 0 & \dots & -E/4 & K \end{bmatrix},$$

where E is a $(N-1)^2$ order unity matrix, and K is a square matrix of order $(N-1)^2$. and

$$K = \begin{bmatrix} 1 & -1/4 & \dots & 0 \\ -1/4 & 1 & -1/4 \dots & \vdots \\ \vdots & \ddots & \ddots & -1/4 \\ 0 & \dots & -1/4 & 1 \end{bmatrix}.$$

For this large scale linear system, the convergence speeds of the Jacobi and Gauss-Seidel iteration methods are very slow. The multi-grid method is an efficient algorithm for accelerating convergence of iterative methods. The scheme alternates between an iteration that quickly reduces local (high frequency) errors, and an approximate solution on a coarse grid for reducing the global (low frequency) error.

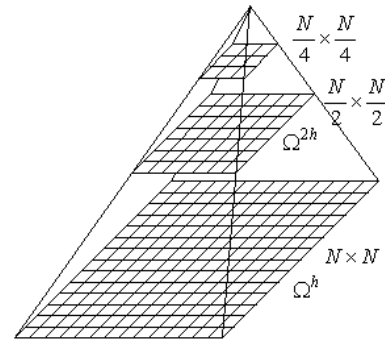


Fig.7 Scheme of the multi-grid algorithm

The iteration procedure is conducted in the pyramid-like structure shown in Fig.7, in which the lowest level is the most refined grid $N \times N$, and grids in higher levels are successively coarser grids. The basic procedure of the multi-grid method is summarized in the following algorithm [13]:

Step 1: On the finest grid space Ω^h , which is the lowest level shown in Fig.7 and whose grid interval is h (we can define it as unity), we relax γ_1 times to solve equation (19) with an initial guess \tilde{U}_0^h and get the approximate \tilde{U}^h .

Step 2: On the coarser grid space Ω^{2h} , which is the second level from the bottom shown in Fig.7 and whose grid interval is $2h$, we solve the residual equation (20) and get the error value v^{2h} . We define I_h^{2h} as a restriction operator for mapping the residual value from fine grid space Ω^h to the coarser grid space Ω^{2h} .

$$L^{2h} * v^{2h} = r^{2h}, \quad (20)$$

Where $r^{2h} = I_h^{2h}(Q^h - L^h * U^h)$, and

$$L^{2h} = I_h^{2h} L^h I_{2h}^h$$

Step 3: In this step, we use the following equation to correct the fine grid solution \tilde{U}^h by the error value v^{2h} :

$$\tilde{U}^h = \tilde{U}^h + I_{2h}^h v^{2h}, \quad (21)$$

Step 4: Backing up to the finest grid Ω^h space, relax γ_2 times to solve equation (19) using the approximate \tilde{U}^h as initial solution and get the solution.

We have solved equation (10) and gotten the matrix U by the multi-grid method. We need to convert the matrix U to a two-dimensional function that presents the reconstructed image \tilde{I} and then crops the two-dimensional function, whose size is $N \times N$, back to the original size $m \times n$. The synthetic image then is reconstructed by the new gradient values, in which there are no outliers, and it can then show clearly the features of the chrome-plated surface.

4. Illumination system

In this section, the illumination system is introduced. The proposed method is based on a set of good original images, therefore, for chrome-plated surfaces the illumination system is a critical point. The Chrome-plated surface is perfectly specular. The specular reflection component reflected off Chrome-plated surfaces is very strong and the diffuse

reflection components are too weak. The intensity of specular reflection often exceeds the limit exposure of the CCD photosensitive surface and results in brightness distortion of the image. These specular reflections will certainly lose the features of the surface and the defect information.

In our experiments, we specially designed the ring illumination system. In the system, a diffuse light source was used and it is shown in Fig.8. The CCD camera was mounted in a fixed position perpendicularly above the observed object. The light source moves in a circular motion at a certain elevation θ while changing its azimuth angle φ .

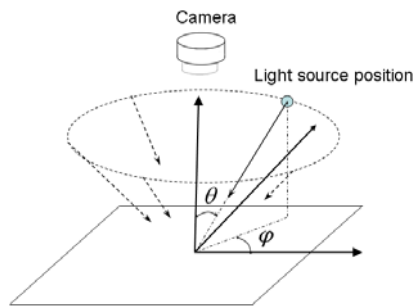


Fig.8 Ring illumination pattern

According to the reflection model shown in section 2, the intensities of the pixels in the image depend on many factors, including the geometric shape, the incident light angle and the luminous intensity, the observation direction of the sensor and the surface optical properties of the object. Different objects require different lighting methods that affect the captured image. For a smooth metallic surface the front lighting method is mostly adopted and consequently the focus is placed on the type of light source.

The light source may be a diffused light source or a parallel light source. Parallel light has strong direction and collimation. The images obtained under parallel light have high contrast and high definition. However their radiance in all directions is not symmetrical, and therefore various defects in different forces occur. Under the same conditions, when the scratches or cracks are perpendicular to the parallel incident light in the direction, the defects present the clearest image. In contrast, if scratches or cracks are parallel to the incident light in the image such defects will be nearly invisible. There is no doubt that this will make the latter image processing very difficult. The diffuse light source achieves non-directional, uniform illumination, resulting in an image with few shadows or highlights. The diffuse illumination of specular reflecting surfaces enables an attenuation of the specular component. But diffuse light may also produce non-distinct edges and low contrast on some surfaces.

Compared with parallel light, diffuse light produces less specular reflection and can present more defect information in the image. Furthermore, for a smooth metallic surface especially Chrome-plated surface defects always appear with high gray values compared to the rest of the surface. So, in our experiment, we select diffuse light as the light source. In so doing we find that only one image cannot describe the complete surface because the specular reflection could result in image distortion so that some information could be lost. On the other hand, the position of the light source also affects the manifestation ability of various defects. References [11] and

[14] discuss the manifestation ability of various defects, and imply better manifestation ability can be obtained when the incidence angle θ is 10-30 [deg].

By selecting a diffuse light source and ring illumination pattern, we can obtain a set of images, and only by using the set of images, we can reduce specular reflection and find all of the defects. In the intact part of a metallic surface, the highlight spots are in different positions. In the defect part of the metallic surface, out of the relation between the direction of the defect and the light source, the spots always appear with different intensities in all images. This illumination system will be of great benefit in reducing specular reflection components and integrating all defects.

5. Experiment Results

This section presents some experimental results of chrome-plated Acrylonitrile Butadiene Styrene resin (ABS resin)[7], which is broadly found in many industries because of its aesthetic appearance.

The experiment system is shown in Fig.9. It is in a dark room in order to eliminate ambient light effects.

The CCD camera, which provides an 8-bit grey level image, was mounted in a fixed position perpendicularly above the observed object. The light source is mounted on a revolving rack. A rotation motor drives the revolving rack in a circular motion which changes the azimuth angle φ .



Fig.9 Experiment system

Figure 10 shows four original gray images of the ABS resin, which were taken with different incidence light directions. The synthetic image is given in Fig.11, which was reconstructed using the proposed method. The histogram of the first image shown in Fig.10 is given in Fig.12. In each original image shown in Fig.10, some pixels are very dark, whose intensities are close to 0, while some pixels are very bright, which are close to or equal to 255 in intensity. This is because, for chrome-plated surfaces, diffuse reflections are very weak and also the specular reflections are very strong. However, it is obvious that the entire surface of the synthetic image appears with medium gray level.

The histogram of the synthetic image is presented in Fig.13. Comparing the two histograms of Figs.12 and 13, it can be observed that the high intensity bright spots have been completely removed from the original image, which has the corresponding histogram spike at pixel value 255.

To evaluate the intensity distribution, we first set a special area which is centered on the intensity line for the peak point

and has a band width $2w$. Then we calculate the intensity percentage in the condition of the different band width w . The relation between the band width w and the intensity percentage is described in Fig.14, where the white square marks show the width w obtained from the histogram of the original image and the black circle marks show the width w obtained from the histogram of the synthetic image. As is shown in Fig.14, after the intensity in the special area rises to more than 95%, the synthetic image has a better distribution than that of the original image. In other words, in a wide area, the intensity distribution for diffuse reflection components becomes worse when removing specular reflection components. This means that the clarity of the synthetic image is better than that of the original image. In addition, the synthetic image histogram has a reduced width as a result of a reduction in the higher pixel values in the main histogram peak.



Fig.10 Four original images taken with different light directions



Fig.11 The synthetic image

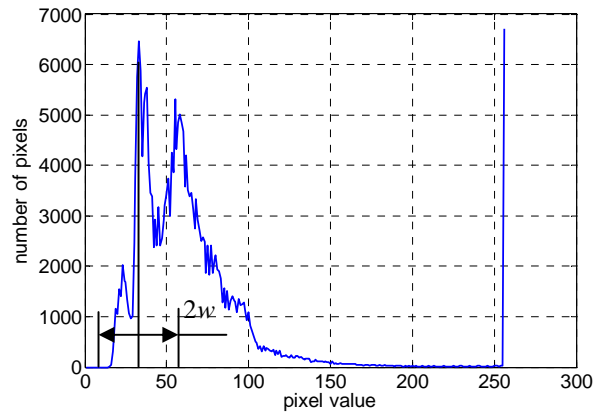


Fig.12 Histogram of the first image of fig 6

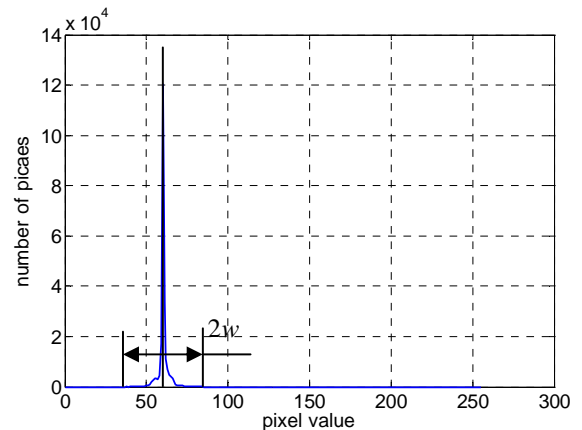


Fig.13 Histogram of the synthetic image

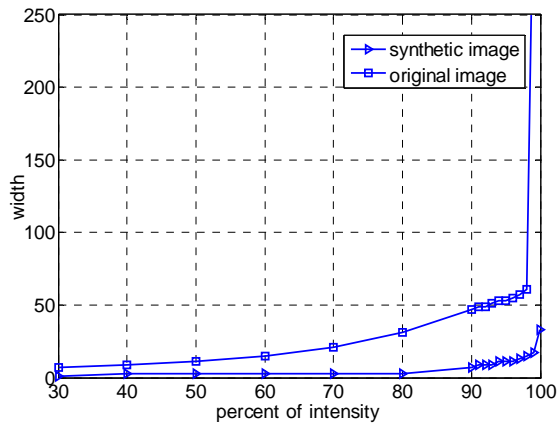


Fig. 14 Intensity distribution between the original image and the synthetic image

Another experimental result can be seen in Fig.15, where four original images were taken from four different incidence light directions. On the part's surface, there are six defects, whose directions and shapes are different. Because four original images were taken from different light directions the defects information have different definitions. For example, in the second image of the first row shown in Fig.15, two defects with horizontal direction do not appear. But the two defects appear clearly in the first image of the second row in Fig.15. In addition, in the first image of the second row in Fig.15, the bottom-left defect appearing in the last image in Fig.15 is hidden in a big specular region. According to our method, we reconstruct the synthetic image, shown in the Fig.16, to reduce specular reflection components and integrate all defects. In the synthetic image, all defects with high intensity compared to the rest of the surface without defect present clearly. We can extract all defects by a simple method of image segmentation, although a defect performance is not too clear. In fact, because of the complication of the defect shape, orientation, and size, more than four images need to be captured. The number of images captured mainly depends on the shape of the object surface and the defect shape. Experiments imply that by using only a set of images we can cover all defect information, particularly for Chrome-plated surfaces.

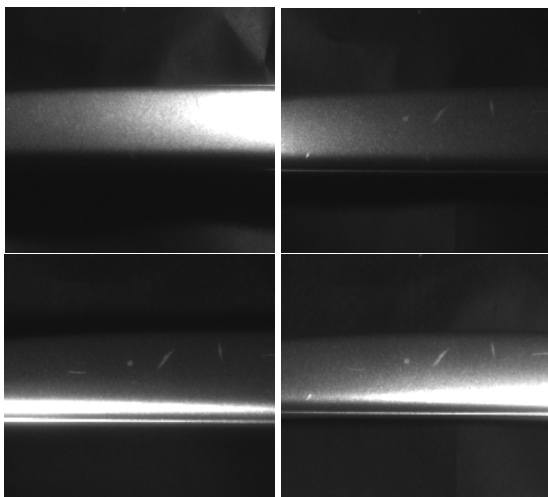


Fig.15 Images of a defect part taken from varying light directions.

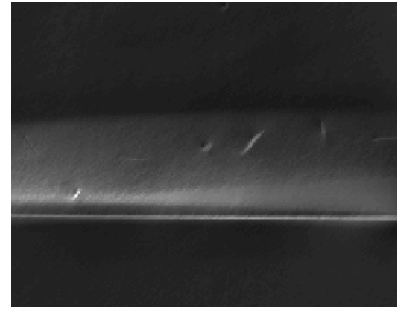


Fig.16 The reconstruction image of a defect part

6. Conclusion and Remarks

A chrome-plated surface is a perfectly specular surface and can be found in many fields because of its aesthetic appearance. The specular reflection component reflected off them is very strong but the diffuse reflection components are too weak. The intensity of the specular reflection often exceeds the limit exposure of the CCD photosensitive surface and results in brightness distortion of the image. Therefore, in one image the complete surface cannot be obtained no matter how it is processed.

To address the problem, this paper proposed a multi-image reconstruction method (MIRM) to achieve complete surface information by processing the specular reflection components. A set of images of the object are captured with different lighting directions and then a synthetic image from the new gradient value calculated from the set of images is reconstructed. In particular we adapt the grid method to reconstruct the synthetic image to ensure the robustness of the method. By processing the synthetic image we can obtain the entire surface. After discussing the reflection model, we designed the illumination system by referring to the reflection model and the properties of the Chrome-plated surface.

We applied the method to the Chrome-plated ABS resin. Compared with the original images, the synthetic image shows some positive changes. (1) The synthetic image histogram has a reduced width around the main histogram peak because of the reduction of those pixels with values that are too high or too low. Also this means the synthetic image has better clarity. (2) The synthetic image appears with medium gray value. But, in the original images some pixels appear too dark or too bright. (3) All defects which cannot be detected in only one original image because of their orientation and shape are integrated in the synthetic image.

Future work will focus on improving the method to increase the precision of the synthetic image. Some parts of the surface present always very dark in every original image. In this case, these parts in the synthetic image cannot have high contrast. It is worthwhile to optimize the correlation parameters of the light source system by investing the relation between the shape and direction of the defect. In addition, further efforts should be made to improve the quality of the gradient image by using the PCA or ICA method. These efforts will certainly be helpful to boost the applicability of the method on the production line.

Acknowledgment

This work was supported by the Global COE Program "Frontiers of Intelligent Sensing" from the Ministry of Education, Culture, Sports, Science and Technology, Japan.

This work was supported in part by Grant-Aid for Scientific Research of the Japan Society for the Promotion of Science. The authors also gratefully acknowledge the helpful comments and suggestions of the reviewers.

References

- [1] L.B. Wolff and T. Boult, "Constraining Object Features Using Polarization Reflectance Model," *IEEE Trans. Pattern Analysis and Machine Intelligence*, vol.13, no.7, pp.635-657, 1991.
- [2] S.K. Nayar, X.S. Fang and T. Boult, "Separation of Reflection components Using Color and Polarization," *Int'l J. Computer Vision*, vol.21, no.3, pp. 163-186, 1996.
- [3] Y. Sato and K. Ikeuchi, "Temporal-Color Space Analysis of Reflection," *J. Optics Soc. Am. A*, vol.11, no.11, pp. 2990-3002, 1994.
- [4] T. Tan Robby and Katsushi Ikeuchi, "Separating Reflection Components of Textured Surfaces Using a Single Image," *IEEE Transactions on Pattern Analysis and Machine Intelligence*, vol.27, no.2, pp.178-193, 2005.
- [5] Rogerio Feris, Ramesh Raskar, K.T.M.T. 2004. Non-photorealistic camera: Depth edge detection and stylized rendering using multi-flash imaging. In *Processing of SIGGRAPH 2004, ACM Press/ACM SIGGRAPH, computer Graphics Proceedings, Annual Conference Series, ACM*.
- [6] Yasuhiro Mukaigawa, Hajime Miyaki, Photometric Image-Based Rendering for Image Generation in Arbitrary Illumination, *Proc. Int. Conf. on Computer Vision*, pp. 643-649, 2001.
- [7] Zhong Zhang, Shiqin Ren, Tetsuo Miyaki, Hisanaga Fujiwara, Takashi Imamura. Processing Reflections on Metallic Surfaces using a Special Random Sampling Method. *International Journal of Innovative Computing, Information and Control*. Volume 4, Number 7, July 2008, pages 1595-1606
- [8] A. Shashua, Geometry and photometry in 3D visual recognition, PhD thesis, Dept. Brain and Cognitive Science, MIT, 1992.
- [9] SK Nayar, Ikeuchi K, Kanade T. Surface reflection: physical and geometrical perspectives. *IEEE Trans. on Pattern Analysis and Machine Intelligence*, vol.13, no.7, pages 611-634, 1991.
- [10] K. E. Torrance and E. M. Sparrow, Theory for off-specular reflection from roughened surfaces, *Journal of the Optical Society of America*, vol. 57, no. 9, pp. 1105-1114, 1967.
- [11] Franz Pernkopf and Paul O'Leary, 'Visual Inspection of Machined Metallic High-Precision Surfaces', *EURASIP Journal on Applied Signal Processing* 2002:7,667-678.
- [12] Yasuhiro Mukaigawa, Hajime Miyaki, Photometric Image-Based Rendering for Image Generation in Arbitrary Illumination, *Proc. Int. Conf. on Computer Vision*, pp. 643-649, 2001.
- [13] Fattal, D. Lischinski. Gradient Domain High Dynamic Range Compression. In *Proceedings of SIGGRAPH 2002*, pages 249-256.
- [14] Garcia-Chamizo, J.M., Fuster-Guillo, A. Visual input amplification for inspecting specular surfaces. *Image Processing, 2006 IEEE International Conference on*; pages 485-488.

Author Biographies



Changjiang LI He received his M.S. degree in mechanical engineering at the University of Science and Technology Beijing, China, in spring 2002. Now he is a doctor student in Toyohashi University of Technology. His research interests include surface inspection, feature selection, and image processing.



Zhong ZHANG He received his Bachelor engineering, Master engineering degrees in 1982 and 1984, respectively, from Xi'an Highway University, China and his Doctor engineering degree in 1993 from Okayama University, Japan. He was a visiting scholar at the University of Melbourne, Australia in 1998. He engaged in research regarding intelligent systems and signals, and image processing as a senior researcher at the Industrial Technology Center of Okayama Prefecture, was an associate professor at Okayama Prefecture University, and is now a professor at the Instrumentation Systems Laboratory of Toyohashi University of Technology.